University of Nebraska - Lincoln

DigitalCommons@University of Nebraska - Lincoln

July 2007

Detection of ultrathin biological films using vacuum ultraviolet spectroscopic ellipsometry

Dileep K. Goyal
University of Nebraska - Lincoln

Greg K. Pribil
J. A. Woollam Co., Inc., Lincoln, NE, USA

John A. Woollam
University of Nebraska-Lincoln, jwoollam1@unl.edu

Anuradha Subramanian
Department of chemical Engineering,University of Nebraska Lincoln., asubramanian2@unl.edu

Follow this and additional works at: https://digitalcommons.unl.edu/cbmesubramanian

Part of the Chemical Engineering Commons

Detection of ultrathin biological films using vacuum ultraviolet spectroscopic ellipsometry

Dileep K. Goyal[a], Greg K. Pribil[c], John A. Woollam[b, c], and Anuradha Subramanian[a,*]

[a] Department of Chemical and Biomolecular Engineering, University of Nebraska–Lincoln, Lincoln, NE 68588, USA
[b] Department of Electrical Engineering, University of Nebraska–Lincoln, Lincoln, NE 68588, USA
[c] J. A. Woollam Co., Inc., Lincoln, NE, USA

* Corresponding author: A. Subramanian — tel 402 472-3463; fax 402 472-6989; email asubramanian2@unl.edu

Abstract

Spectroscopic ellipsometry (SE) is a non-contact and a non-destructive optical technique used in characterization of thin films. It is widely used to determine optical constants, thickness in multilayer stacks and microstructure (voids, alloy fraction, or mixed phase composition). This paper reports on a systematic investigation of the optical properties of two different kinds of silane compounds: 3-aminopropyltriethoxysilane (APTES) and 3-glycidoxypropyltriethoxy-silane (GPS) as well as for immunoglobulin G (IgG) attached to these modified samples using vacuum ultraviolet spectroscopic ellipsometry (VUV-SE). VUV-SE is a newly developed technique and used to evaluate the strength and energy of the interband electronic excitations/transitions in these biofilms. The shorter wavelengths of VUV-SE increase sensitivity for detection of extremely thin adsorbed films at an interface (<10 nm) and accurately determine optical properties of biological interactions/moieties on the surface. A Cauchy dispersion model was used to determine layer thicknesses in multilayer stacks and adsorption was accounted by including Gaussian shaped oscillators in the optical model. No measurable optical anisotropy is found for these films. The dielectric properties of the adsorbed films are reported in the 0.73–9.43 eV optical range.

Keywords: silane, ellipsometry, human immunoglobulin, vacuum ultraviolet, oscillators

1. Introduction

Characterization of adsorbed biomolecules (e.g. nucleic acids and proteins) on solid surfaces plays an important role in the study of various biological processes relevant to biorecognition, bioseparations and biosensing. To make quantitative gains in sensitivity and selectivity at the nanoscale level, it is very desirable to develop techniques and tools to enable detection and identification of adsorbed molecules on biofunctionalized surfaces. In most cases resolution and detection of these events are desired at the monolayer level, i.e. less than 10 nm. It is also desired to obtain important information about the thickness and surface coverage of adsorbed monolayers, biomolecules as well as molecular concentration to understand the biomolecule–material interactions at the surface. Techniques employed to evaluate and quantify biological interactions at solid surfaces include assays using fluorescent, radiolabelled, or immunochemical detection tags and optical techniques such as ellipsometry, infrared (IR) spectroscopy and Raman spectroscopy. While optical techniques offer the advantage of being non-destructive and non-contact bearing, most optical methods require an accurate knowledge of optical properties of the materials to enable an accurate description of the interaction of radiation with the material [1].

Obtaining optical properties of materials such as metals, organic films, and biological moieties such as ligands, peptides, DNA and proteins in the wide spectral range has been a challenge. Previous research has shown that high quality measurements can be performed on metals and organics over a wide range of energies from visible to X-ray regions to study the optical properties [2] and [3]. There is a need to determine the optical properties of many biological moieties and biofunctionalized surfaces in spectral regions ranging from vacuum ultraviolet (VUV) through soft X-ray regions. Techniques such as electron energy loss spectroscopy [4] and [5], ellipsometry [6], the angle dependence of the photoelectric yield [7], and interferometry [8] are used for deriving the optical properties of materials in the VUV through X-ray regions. However the

optical properties of protein monolayers, ultrathin organo-silane monolayers (<10 nm) on solid surfaces are not known. Many molecules absorb UV radiations and corresponding absorption bands represent structural groups known as chromophores within the molecule. VUV-SE shows higher sensitivity towards the detection and identification of biomolecular interactions at the monolayer level as light in the VUV range is higher in energy and thus has a short penetration depth into materials which makes VUV-SE higher in surface sensitivity for extremely thin adsorbed films [9] and [10]. With shorter penetration depth, VUV-SE is capable of addressing these issues for ultrathin films and a brief summary of optical properties of studied biofilms in wide spectral range (i.e. 0.73–9.43 eV) using VUV-SE is presented.

In literature, researchers have used VUV-SE to investigate: (a) interband optical properties of crystalline (quartz) and amorphous SiO_2 [11], (b) optical properties of thin silicon oxynitride film with thickness 25–35 nm [12], (c) direct observation of the dielectric properties of cubic SiC from electronic transitions [13], (d) optical and electronic properties of amorphous carbon films [13] and [14], (e) electronic structure of complex oxides such as high k dielectrics [15], [16], [17], [18], [19] and [20], (f) optical properties of binary transition metal (TM) nitrides and carbides [21], (g) optical constants of lithography based films (photoresists, AR coatings, etc.) and Alq_3 thin films for large-area display applications [22] and (h) optical and electronic properties of high refractive index materials such tantalum oxide thin films [23]. Dielectric properties of DNA base films, i.e. guanine, adenine, cytosine, and thymine in the energy range from near-IR to UV have been investigated using VUV-SE. The imaginary part of the dielectric properties ε_2 of the DNA base films was compared to the electronic transitions of single molecules calculated using time dependent density function theory [24], [25] and [26]. The photophysical and photochemical behavior of the organic molecules such as phenylsilane on silicon was also studied by VUV-SE [27]. In the presented work, we used VUV-SE to detect and identify biological moieties/interactions present at a solid interface of extremely thin adsorbed films and also to accurately determine optical properties of the adsorbed monolayers.

2. Materials and methods

Polished silicon wafers (2 in. diameter (100), *p*-type, resistivity (p) < 0.1) were purchased from Polishing Corporation of America (Santa Clara, CA). Sulfuric acid (ACS Plus grade) and Hydrogen peroxide (ACS grade 30% solution) was purchased from Fisher Scientific (Pittsburgh, PA). Sodium hydroxide pellets (ACS reagent) were purchased from Sigma (St. Louis, MO). Ethanol (200 proof) was purchased from AAPER Alcohol (Shelbyville, KY). 3-Aminopropyltriethoxysilane (APTES) and 3-glycidoxypropyltriethoxysilane (GPS) were purchased from Gelest, Inc. (Morrisville, PA). Chemicals used for the buffer (PBS, pH 7.4) preparation were all of analytical grade or better. Glutaraldehyde (70% aqueous solution) and ethanolamine were purchased from Sigma–Aldrich (St. Louis,

MO). Human IgG (lyophilized powder) was obtained from Equitech Bio, Inc. (Kerrville, TX). Deionized water was obtained from a Millipore milli-Q ion exchange apparatus. All chemicals were used as purchased without further purification.

2.1. Cleaning of silicon wafers

Silicon wafers were cut into 1 cm^2 pieces and cleaned by sonication in ethanol (200 proof) for 20 min. Wafers were hydroxylated using mixture of 30% hydrogen peroxide (H_2O_2) and concentrated sulfuric acid (H_2SO_4) (1:3, v/v) for 30 min [28]. After neutralizing with NaOH (2 M) for 3 min, samples were thoroughly rinsed with water for 15 min. Cleaned samples were stored in DI water before use.

2.2. Silanization of cleaned silicon wafer surfaces with APTES

Cleaned wafers were reacted with a fresh 1% (v/v in ethanol) APTES solution for 15 min under N_2 atmosphere at room temperature. Upon reaction completion, the wafers were rinsed three times with pure ethanol, and then sonicated in pure ethanol for 15 min to remove any non-covalently bonded silane compounds. Samples were baked for 15–20 min at 70–75 °C to stabilize the silane monolayer on silicon wafers.

2.3. Silanization of cleaned silicon wafer surfaces with GPS

Cleaned wafers were reacted using a fresh 1% (v/v in ethanol) GPS solution for 60 min under N_2 atmosphere, at room temperature. Upon reaction completion, the wafers were rinsed three times with pure ethanol, and then sonicated in ethanol for 15 min to remove any non-covalently bonded silane compounds. Samples were baked for 15–20 min at 70–75 °C to stabilize the silane monolayer on the silicon wafers. This process renders epoxy terminated surfaces which allows us to immobilize protein without using crosslinking agents.

2.4. Covalent immobilization of Human IgG

In this paper, silicon surfaces modified with APTES were reacted with a 2.5% glutaraldehyde solution in PBS buffer (pH 7.4) for 6 h [28], followed by rinsing with PBS buffer and DI water three times. The glutaraldehyde activated and epoxy terminated surfaces were then placed into 1.0 mg/ml Human IgG solution at room temperature for 24 h with moderate shaking speed. The surfaces were washed with PBS buffer (pH 7.4) and DI water. Surfaces were dried using N_2 gas before measurement.

2.5. Ellipsometry

A Commercial Vacuum Ultraviolet Variable Angle Spectroscopic Ellipsometer with photon energy range (0.73–9.43 eV) and using two angles of incidence (65° and 75°) were used. Ultraviolet light is obtained from a deuterium (D_2) lamp combined with Xe lamp for spectral coverage to longer wavelengths. The ellipsometer utilizes double chamber monochromator improved stray-light rejection in addition to wavelength selection and slit-width control. The monochromator was placed before the sam-

ple to avoid exposure of photo-sensitive materials. Highly accurate measurements were taken on each sample using an AutoRetarder®. Depolarization effects were separated from the optical constant measurements using the AutoRetarder®, as the measurements were based on Mueller-matrix elements rather than Jones-matrix elements [29]. A vacuum ambient is not required for the spectral range up to 10 eV. Instead, the ambient is purged using dry nitrogen to avoid adsorption from oxygen and water vapor prominent above 6.5 eV. Optical modeling of all measured data was carried out using commercial software. All the measurements were done in dry state of samples.

3. Data analysis

In this section, a brief description of the data modeling process is presented and the strategy adopted to model the VUV data is also included. An ellipsometer yields two measurable quantities, Psi (Ψ) and Delta (Δ), at each wavelength and angle of incidence, which describes the change in the polarization state of light when it is allowed to interact with the sample under investigation [1]. Ellipsometry does not measure optical constants or film thickness directly; however Psi (ψ) and Delta (Δ) can be represented as mathematical functions relating these material characteristics. Hence, a mathematical analysis called a model-dependent analysis must be performed to determine real parameters from the measured ellipsometric data. Numerous material parameters can potentially be determined through spectroscopic ellipsometry analysis, including layer thickness, surface and/or interfacial roughness, optical constants, and void fraction [30], [29] and [31], using optical physics (Fresnel reflection coefficients, Snell's law, etc.). The modeling process is illustrated in Figure 1 (adapted from http://www.jawoollam.com).

Most dielectric materials are transparent in visible spectral wavelengths and become adsorbing in the higher VUV photon energy range [32]. A simple dispersion relation is often used to describe optical properties for many materials in non-adsorbing regions for dielectrics and semiconductors, but not metals [33] and [34]. The Cauchy–Urbach relationship represents the index of refraction n and extinction coefficient k as slowly varying functions of wavelength, λ, with an exponential to

Figure 1. Modeling process using WVASE software.

represent a short wavelength absorption tail:

$$\eta = A + \frac{B}{\lambda^2} + \frac{C}{\lambda^4} \tag{1}$$

$$k = A_k \exp \beta_k (E - E_b) \tag{2}$$

where A, B, and C are known as the *Cauchy Coefficients*. A gives the constant value of 'n' at long wavelengths, B controls the curvature of 'n' in the middle of the visible spectrum and C influences the spectrum to a greater extent for shorter wavelengths. The extinction coefficient 'k' is expressed as a function of the photon energy in the Urbach relationship, i.e. Eq. (2). In this equation, 'k' is expressed in terms of the extinction coefficient amplitude A_k, the exponent B_k, and the band edge E_b. These parameters (except E_b, fixed at short wavelength) can be defined as fit parameters in the Cauchy layer to perform model-dependent analysis. The initial values for these parameters used in this study were approximately valid for thermal silicon oxide [30]. ($A = 1.45$; $B = 0.01$; $C = 0$; $A_k = 0$; $B_k = 1.5$; $E_b = 3.1$ eV.)

However, a different model, an oscillator model, was needed to describe the film absorption at shorter wavelengths, i.e. at higher photon energies. Gaussian shaped oscillators were used to incorporate the effect of adsorption in the VUV spectral range. Dielectric properties for the Gaussian shaped oscillators are shown below [34]:

$$\in_{2G}(E) = A \exp \left[-\frac{(E - E_c)^2}{B^2} \right] \tag{3}$$

$$\in_{1G}(E) - K\{\in_{2G}(E)\} \tag{4}$$

where, A is the amplitude, E_c is the center energy, B is the broadening and K represents the Kramers–Kronig transformation in Equations (3) and (4).

There are two common modeling approaches used to describe optical properties for films transparent in the visible but that absorb in VUV spectral range: the wavelength-by-wavelength (λ-by-λ), or point-by-point approach and the oscillator model approach. Both methods start by fitting measured data in the transparent region to determine film thickness. In the λ-by-λ approach, the resulting thickness is fixed to determine optical properties 'n and k' from the measured quantities 'ψ and Δ' and the oscillator model approach describes the optical constants using a dispersion relation taking the absorption into consideration. The parameters of this relation can be varied to fit the experimental data and can be used to evaluate the characteristic of the studied material. Most oscillator models maintain Kramers–Kronig consistency hence it is reasonable to assume that the resulting optical constants maintain a physical shape.

In this study, these two approaches were combined for further benefit. The data were acquired over the desired spectral range (0.73–9.43 eV) and angles of incidence (65° and 75°) and the following procedure used to analyze all data. First, to determine the film thickness of each sample, a model was constructed in the transparent region, used from wavelength 350 to 1200 nm) based on the nature and chemistry of the thin films as well as the Si substrate properties. For most transparent films, the value of k is equal to zero and hence Urbach relation was
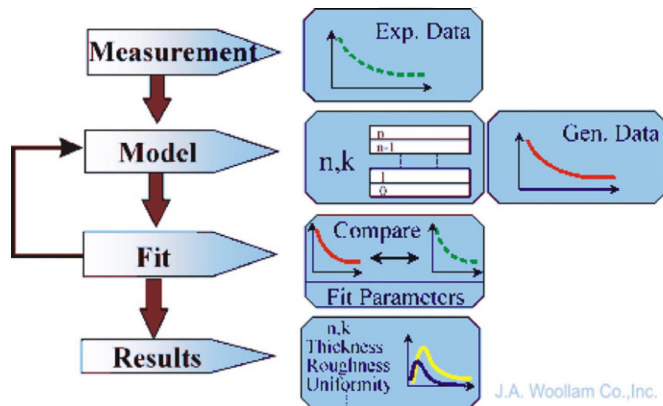
only included to model the onset of UV absorption. Optical constants of silicon substrates were taken from the literature [35]. A standard oscillator model for SiO₂ was used to describe optical properties of both the oxidized and hydroxylated silicon layer for all the samples. Cauchy dispersion relations were used to describe the optical properties of the APTES monolayer, GPS monolayer and Human Immunoglobin G (HIgG) film in the respective samples. In case of a combination of two layers in a sample (e.g. APTES and HIgG), both Cauchy layers were not coupled to each other but were fitted separately to identify optical constants of each film. Second, the assumed model was used to generate the expected Ψ and Δ for the selected wavelength range and angles of incidence. Lastly, the measured 'Ψ and Δ' data were compared to the model-based generated 'Ψ and Δ' data. Iterations of a fitting algorithm were then performed to adjust the selected model parameters so that the model-predicted Ψ and Δ data match the measured ones as closely as possible. The most commonly used algorithm is the Marquart–Levenberg algorithm [36]. The closeness of the fit is described by the Mean Square Error (MSE), which is used to quantify the difference between the experimental and generated data [37]. A lower MSE implies a better fit.

Here, the model-dependent analysis was done in two sections. In the first section, to determine the film thickness, a Cauchy layer model was used to describe optical properties of the silane and protein monolayer in the user selected transparent region (i.e. 350–1200 nm). The thickness and Cauchy parameters were used as fitting parameters in the model. In the second section, the resulting thickness was fixed to determine the sample optical properties in the adsorbing region. In this section, a λ-by-λ approach was used to fit the data from the assumed model in the selected spectral range from 3.5 to 9.43 eV. Optical constants resulting from the λ-by-λ approach were then used as a reference material in a general oscillator layer. New Gaussian shaped oscillators were added to the general oscillator layer to obtain a new dispersion relation. Both ε_1 and ε_2 generated by this dispersion relation were fitted to the reference material and the resulting dispersion relation was used to generate ψ and Δ data and compare with experimental ψ and Δ data. The number of oscillators and oscillator parameters such as center energy, broadening and amplitude, etc. were adjusted to match the experimental data and this procedure was iterated until a best fit was obtained. Once the best fit was obtained, resulting material optical constants were saved and the various oscillator strengths, energy and broadening were tabulated. Oscillator models used here are Kramers–Kronig consistent hence it is reasonable to assume that resulting optical constants maintain a physically meaningful shape. Last, the newly obtained model was fitted against experimental data for the entire spectral range.

4. Results and discussion

As a case study, five samples were examined using VUV-SE. A cleaned silicon surface, APTES (3-aminopropyltriethoxysilane) monolayer grafted silicon surface, Human IgG immobilized on APTES grafted surface using glutaraldehyde, GPS (3-glycidoxypropyltriethoxysilane grafted silicon surface and Human IgG immobilized on GPS grafted surface corresponding to sample 1, 2, 3, 4 and 5, respectively. After hydroxylation or piranha treatment (i.e. sample 1), silicon native oxide thickness was reduced to 2.087 from 2.5 nm. A Cauchy layer was added to this basic model to represent the APTES layer grafted onto the hydroxylated silicon surface. The molecular length of the APTES molecule, shown in Figure 2, was calculated using an optimized geometry experiment in the computer-aided chemistry software BioMedCACHe® by Fujitsu and was found to vary from 0.6 to 1.0 nm depending on the orientation. Thus, it is reasonable to assume that the expected increment in average thickness after a monolayer deposition of APTES should be in a similar range. Using Cauchy layer, the fitting procedure results in APTES layer thickness (i.e. Cauchy layer thickness) equal to 1.496 nm. The average thickness of a silane layer is in the range of monolayer and thus it can be assumed that sample 2 (i.e. APTES grafted surface) has either monolayer or double layer of APTES molecules grafted on to the surface, but not multilayers. Similarly, the thickness of the GPS layer in sample 4 was found to be 0.211 nm. The molecular length of GPS molecule, shown in Figure 2, was calculated by using computer-aided chemistry software BioMedCACHe® and found to be in the range of around 0.9–1.1 nm, thus it indicates that sample 4 (i.e. GPS grafted surface) is partially covered with GPS molecules and does not have any multilayer formation on the surface. An optical model for sample 3 was constructed by adding a Cauchy layer to the previous model, to describe the optical properties of protein immobilized surfaces. Human IgG antibody molecules have a nominal size of 7.0–8.0 nm when attached vertically and ~3.0–4.0 nm when inclined completely [38] so depending on the structure of antibody on surfaces, measured thickness is an average. Thickness data shown in Table 1 confirms attachment of Human IgG on both APTES and GPS grafted surfaces (i.e. samples 3
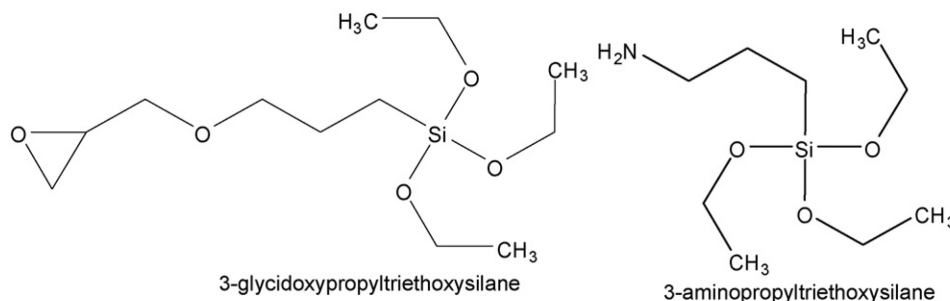

Figure 2. Molecular structure of GPS (3-glycidoxypropyltriethoxysilane) and APTES (3-aminopropyltriethoxysilane) compounds.

Table 1. Sample description and film thickness determined using Cauchy dispersion relation in the transparent region

Sample no.	Description	Thickness (nm)		
		SiO$_2$	Silane	HIgG
1	Hydroxylated or clean silicon wafer	2.087	–	–
2	APTES grafted surface (1%, v/v APTES solution)	2.087	1.496	–
3	Human IgG immobilized on APTES grafted surface using glutaraldehyde as crosslinking agent	2.087	1.496	4.809
4	GPS grafted surface (1%, v/v GPS solution)	2.087	0.211	–
5	Human IgG immobilized on GPS grafted surface	2.087	0.211	3.409

and sample 5). Samples 3 and 5 show an increment of thickness, i.e. 4.81 nm and 3.41 nm after Human IgG immobilization, respectively. The thickness data presented in this article is an average over 1 cm^2 of surface, and the surface coverage of respective layers has not been studied in this article.

After determining film thicknesses for each layer in all samples, combination of both wavelength-by-wavelength (λ-by-λ) approach and the oscillator model approach was used to determine optical properties of APTES, GPS and Human IgG layer on silicon surfaces in the VUV range. Gaussian oscillators and their parameters such as center energy, broadening and amplitude were used to fit the peaks obtained by the wavelength-by-wavelength approach. In all samples several noticeable chemistries were seen in the VUV data. Detectable chromophores or compounds using VUV spectroscopy are shown for reference in Table 2 [39].

Figure 3 shows the real and imaginary part of dielectric properties (ε_1 and ε_2) of APTES film as a function of photon energy from 0.73 to 9.43 eV. Table 3 corresponding to sample 2, shows the oscillator parameters: amplitude, center energy (in eV) and broadening of oscillator's peaks, obtained for APTES film. The features at center energies 6.4501 and 8.73 eV can be assigned to C–N ($n \rightarrow \sigma^*$ transition) and C–C Sigma bond chromophores, respectively. Sigma bond chromophores show the result of adsorption due to σ to σ^* excitations. Similarly, Table 3 corresponding to sample 4 shows the oscillator parameters obtained for GPS film. It is of most importance to point out the feature at approximately 7.37 eV in Figure 4 for the GPS-modified sample. GPS contains an epoxy group in the molecule and absorption due to it can clearly be seen in

the data. Peaks at central energies 8.69 and 8.83 eV in Figure 4 can be assigned to C–C Sigma bond chromophores for the GPS-modified sample. Figure 5 compares the real and imaginary part of dielectric properties (ε_1 and ε_2) of APTES and GPS films as a function of photon energy. Because it is only the GPS-modified surface which contains an epoxy group, the feature at 7.37 eV is present in the curve of the GPS-modified sample. Similarly, the C–N chromophores or C–NH$_2$ peak at 6.4501 eV is only present in the APTES-modified sample since the APTES molecule contains an –NH$_2$ group in chains. The C–C Sigma bond chromophore peaks are present in both APTES and GPS-modified sample. Features present in the 3–4 eV range might be due to the silicon substrate. The real and imaginary parts of dielectric constants for silicon substrates
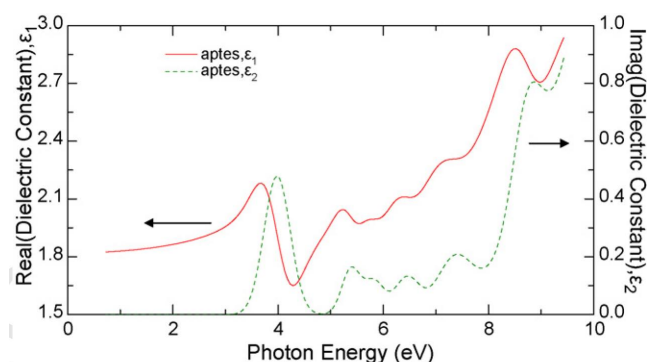
Figure 3. Optical properties (ε_1 and ε_2) for APTES monolayer (sample 2) determined by fitting oscillator model to experimental data in complete spectral range (0.73–9.43 eV, i.e. $\lambda = 1240$/ev, nm).

Table 2. Spectral table to determine organic compounds in VUV region

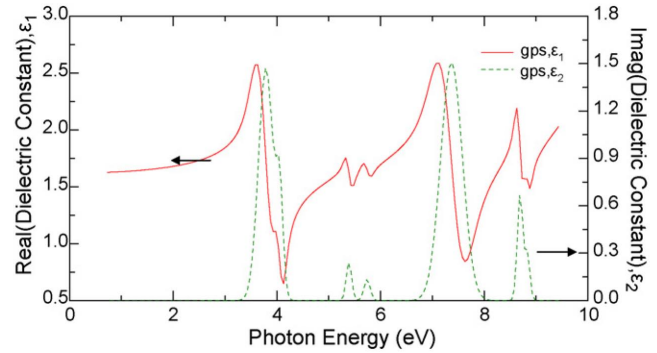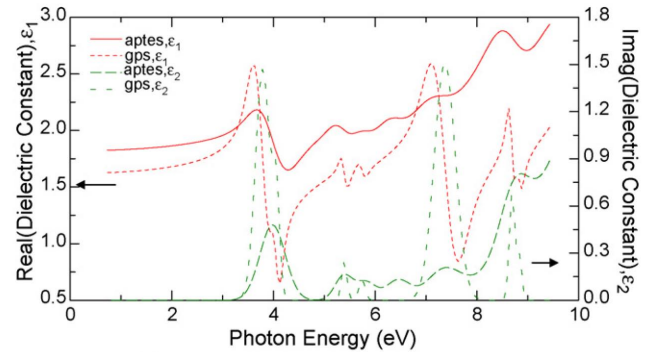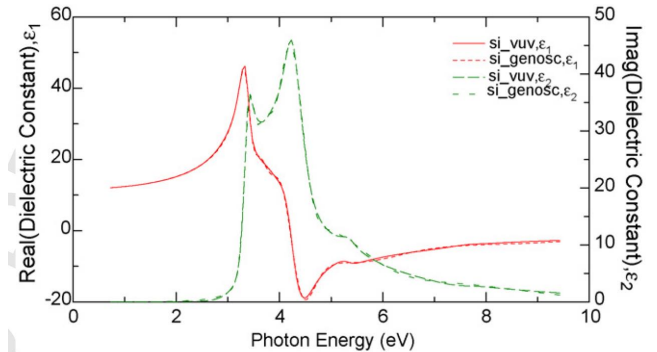| Chromophore	Compound type	Transition	Log ε	Wavelength (nm)	Energy (eV)
	Epoxy	$n \rightarrow \sigma^*$	3.6	166.7–175	7.09–7.45
	R–O–R	$n \rightarrow \sigma^*$	3.5	183.33	6.775
	R–NH$_2$	$n \rightarrow \sigma^*$	3.5	191.67–200	6.21–6.48
	R–COOH	$n \rightarrow \pi^*$	1.7	200–216.67	5.73–6.21
Molar absorptivity (ε)					
C–C	CH$_3$–CH$_3$	$\sigma \rightarrow \sigma^*$	Strong	135	9.2
C–H	CH$_4$	$\sigma \rightarrow \sigma^*$	Strong	122	10.180
C–O	CH$_3$–OH	$n \rightarrow \sigma^*$	200	177	7.017
	CH$_3$–O–CH3	$n \rightarrow \sigma^*$	2500	184	6.75
C–N	(C$_2$H$_5$) 2NH	$n \rightarrow \sigma^*$	2500	193	6.435
	(CH$_3$) 3N	$n \rightarrow \sigma^*$	4000	199	6.241
C=O	CH3–COOH	$n \rightarrow \pi^*$	50	200	6.21
	CH3–CONH2	$n \rightarrow \pi^*$	63	220	5.646

This table lists common organic chromophores and the approximate location of their absorption maxima with associated molar absorptivity (ε). The values reported above, are from tabulated data obtained through the study of compounds in the gaseous or liquid state and not from the solid state.
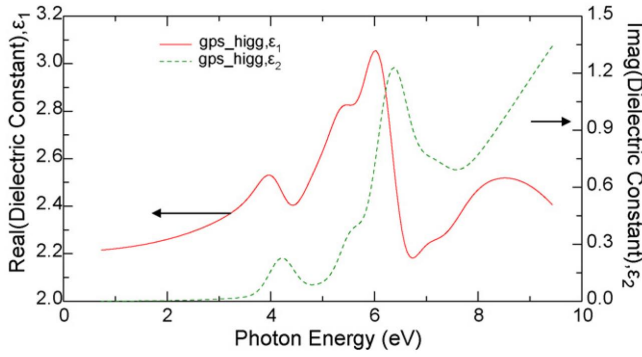
Table 3. Gaussian oscillator parameters for different type of surfaces in the VUV region

Surface type	Amplitude	Energy (eV)	Broadening (eV)
Silicon substrate	19.497	3.407	0.203
	24.819	3.662	0.515
	34.295	4.211	0.530
	10.855	4.770	1.933
APTES	0.480	3.981	0.586
	0.379	8.737	0.660
	3.322	12.101	3.840
	0.122	6.450	0.544
	0.154	5.379	0.403
	0.113	5.813	0.461
GPS	1.472	3.788	0.337
	0.615	4.054	0.151
	0.244	5.390	0.123
	1.335	5.741	0.142
	1.508	7.370	0.491
	0.682	8.692	0.125
	0.298	8.834	0.110
	43.209	11.748	0.173
HIgG on APTES	0.061	5.493	0.339
	0.697	6.347	0.635
	0.475	7.042	1.761
	0.163	7.099	8.054
	1.088	9.416	2.769
	15.223	12.663	0.796
HIgG on GPS	0.183	4.205	0.551
	0.197	5.545	0.490
	0.895	6.329	0.680
	0.273	7.005	0.843
	1.833	11.558	6.347

Figure 4. Optical properties (ε_1 and ε_2) of GPS monolayer (sample 4) determined by fitting oscillator model to experimental data in complete spectral range (0.73–9.43 eV, i.e. $\lambda = 1240$/ev, nm).

Figure 5. Optical properties (ε_1 and ε_2) of APTES and GPS monolayer determined using Oscillator model for complete spectral range (0.73–9.43 eV, i.e. $\lambda = 1240$/ev, nm).

Figure 6. Optical properties (ε_1 and ε_2) of Silicon determined by VUV ellipsometry (si_vuv) and by a general oscillator model (si_genosc) in spectral range (0.73–9.43 eV, i.e. $\lambda = 1240$/ev, nm).
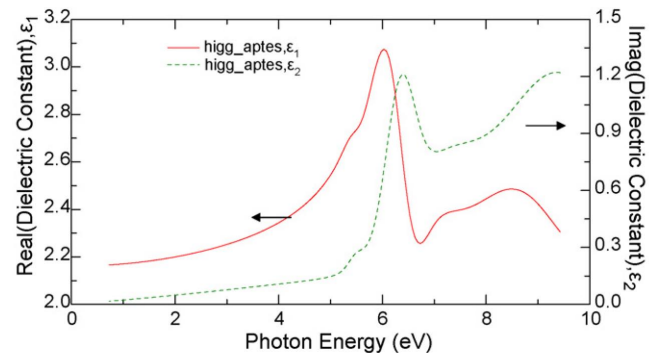
Figure 7. Optical properties (ε_1 and ε_2) of HIgG on APTES grafted surface (higg_aptes) determined by fitting oscillator model to experimental data in complete spectral range (0.73–9.43 eV, i.e. $\lambda = 1240$/ev, nm).

are shown in Figure 6. Since the APTES and GPS-modified surface thicknesses are very low compared to the penetration depth in the VUV, substrate features are still present in the optical properties of APTES and GPS films. For thicker samples, these substrate features are comparatively subdued. Specifically, since the GPS layer thickness was observed to be very low, it is uncertain to obtain absolute index values. However, it is reasonable to assume that the spectral features present are valid since it disappears after protein immobilization. This is also supported by the fact that substrate features are quenched in Figure 7 and Figure 8 which shows optical properties of Immobilized Human IgG layers on APTES and GPS grafted surfaces (i.e. samples 3 and 5), respectively. Due to limited knowledge of chromophores in the VUV range, some of features could not be assigned in the observed data.

Table 3 also show oscillator parameters for Immobilized Human IgG layers on APTES and GPS grafted surfaces (i.e. samples 3 and 5), respectively. In Table 3, features at center energies 5.49, 6.35, 7.0 and 9.4 eV (shown in Figure 7) can be assigned to C=O ($n \rightarrow \pi^*$ transition), C–N, C–O ($n \rightarrow \sigma^*$ transition), C–C ($\sigma \rightarrow \sigma^*$ transition) chromophores, respectively. Similar features are also present for sample 5 (i.e. Human IgG immobilized on GPS grafted surface) seen in Figure 8 at center

Figure 8. Optical properties (ε_1 and ε_2) of HIgG on GPS grafted surface (gps_higg) determined by fitting oscillator model to experimental data in complete spectral range (0.73–9.43 eV, i.e. $\lambda = 1240/ev$, nm).
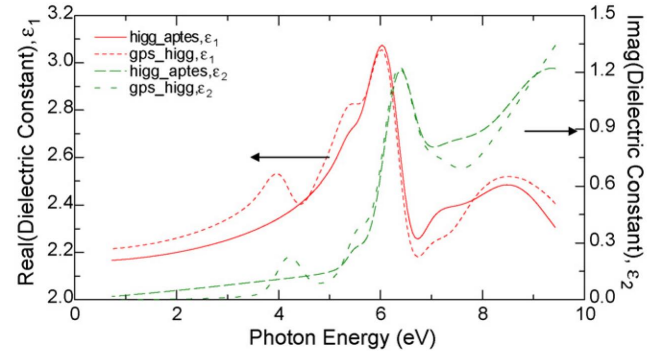
Figure 9. Optical properties (ε_1 and ε_2) of HIgG on APTES (higg_aptes) and GPS (gps_higg) grafted surface determined using Oscillator model for complete spectral range (0.73–9.43 eV, i.e. $\lambda = 1240/ev$, nm).
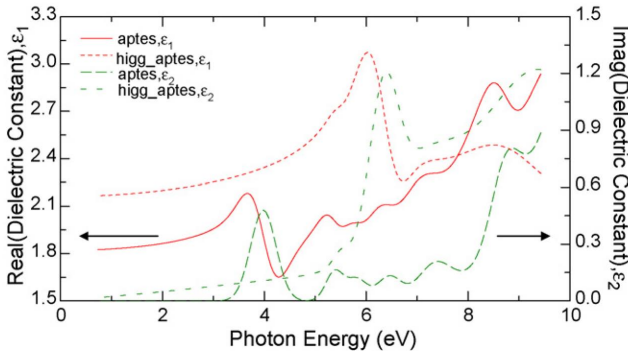
Figure 10. Optical properties (ε_1 and ε_2) of APTES monolayer and HIgG on APTES (higg_aptes) grafted surface determined using Oscillator model for complete spectral range (0.73–9.43 eV, i.e. $\lambda = 1240/ev$, nm).
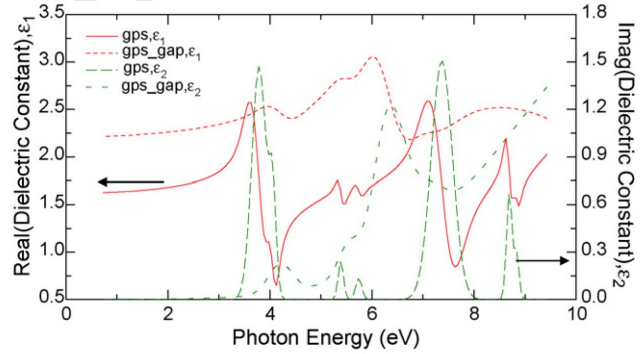
Figure 11. Optical properties (ε_1 and ε_2) of GPS monolayer and HIgG on GPS (gps_higg) grafted surface determined using Oscillator model for complete spectral range (0.73–9.43 eV, i.e. $\lambda = 1240/ev$, nm).

energies 5.55, 6.33 and 7.0 eV (Table 3). Figure 9 compares optical properties of Human IgG immobilized on APTES and GPS grafted surfaces, respectively. It can be observed that both the curves look very similar to each other, as expected.

Figure 10 compares dielectric constants of APTES and Human IgG simultaneously immobilized on an APTES grafted surface. It can be observed that the feature present around 6.35 eV due to C–N ($n \rightarrow \sigma^*$ transition) chromophores becomes stronger. It is known from literature that Human IgG, i.e. proteins, have C–N bonds in abundance. Similarly, compare GPS and Human IgG immobilized on GPS grafted surfaces in Figure 11. Note that the feature at 7.37 eV due to the epoxy group in GPS molecule is quenched, and a feature at 6.32 eV appears due to the presence of C–N bonds in proteins. It is important to note that energy assignments are approximations because values were taken from tabulated data obtained through the study of compounds in the gaseous or liquid state and not from the solid state [39].

5. Conclusions

In summary, we have shown that the isotropic dielectric properties of thin silane and protein monolayers can be determined by spectroscopic ellipsometry from the near-IR to VUV spectral range. The spectra were modeled using a Cau-

chy dispersion relation in visible range and Gaussian shaped oscillators incorporate adsorption features in the VUV range. These models provide a good description of the acquired spectra and accurately identify the molecules on the surface. The adsorption spectrum of two different compounds: 3-aminopropyltriethoxysilane and 3-glycidoxypropyltriethoxysilane and the spectra of immobilized Human IgG on silicon surfaces were analyzed based on certain distinguishable chromophores present in the molecules. A comparative study of APTES and GPS grafted surfaces points out that adsorption peaks at 6.45 eV and 7.37 eV are due to presence of C–N chromophores or C–NH$_2$ and epoxy groups in respective molecules. The absorption peak present due C–N chromophores on APTES grafted surfaces become strong when Human IgG is immobilized on these surfaces. Similarly, the adsorption peak at 7.37 eV due to the epoxy group on the GPS grafted molecule is quenched when Human IgG is immobilized on these surfaces, and feature appears at 6.32 eV due to the presence of C–N bonds in proteins. Accurate dielectric properties of organic/biofilms were obtained in the energy range from 0.73 to 9.43 eV. In conclusion, VUV-SE shows great promise for determining surface chemistry due to the relatively shallow light penetration depth. This depth depends on the extinction coefficient value for each particular adsorption.

References

[1] R.M.A. Azzam and N.M. Bashara, Ellipsometry and Polarized Light, North-Holland, New York (1987).

[2] E.M. Gullikson In: J.A.R. Samson and D.L. Ederer, Editors, *Vacuum Ultraviolet Spectroscopy I*, Academic Press, San Diego (2000), pp. 257–269.

[3] E.D. Palik, Handbook of Optical Constants of Solids, Academic Press, New York (1998).

[4] H. Raether, Excitation of Plasmons and Interband Transitions by Electrons, Springer Berlin/Heidelberg, Berlin (1980).

[5] S.E. Schnatterly In: H. Ehrenreich, F. Seitz and D. Turnbull, Editors, *Solid State Physics*, Academic Press, New York (1979), pp. 275–358.

[6] E.D. Palik, Handbook of Optical Constants of Solids II, Academic Press, New York (1991) pp. 213–246.

[7] H.-G. Birken, C. Blessing, C. Kunz and R. Wolf, *Rev. Sci. Instrum.* **60** (1989), pp. 223–226.

[8] J. Svatos, D. Joyeux, D. Phalippou and F. Polack, *Opt. Lett.* **18** (1993), pp. 1367–1369.

[9] J.N. Hilfiker In: H.G. Tompkins and E.A. Irene, Editors, *Handbook of Ellipsometry*, William Andrew Inc. (2005), pp. 721–762.

[10] W.H. Nosal, University of Nebraska–Lincoln, 2006.

[11] G.L. Tan, M.F. Lemon, D.J. Jones and R.H. French, *Phys. Rev. B* **72** (20) (2005), pp. 205117/1–205117/10.

[12] H.J. Kim, Y.J. Cho, H.M. Cho, S.Y. Kim, C. Moon, G. Cho, Y. Kwon, in: D.G. Seiler, A.C. Diebold, T.J. Shaffner, R. McDonald, S. Zollner, R.P. Khosla, E.M. Secula (Eds.), American Institute of Physics, 2003, pp. 171–175.

[13] S. Logothetidis, H.M. Polatoglou, J. Petalas, D. Fuchs and R.L. Johnson, *Physica B* **185** (1993), pp. 389–393.

[14] S. Logothetidis, *Diamond Relat. Mater.* **12** (2003), pp. 141–150.

[15] C.C. Fulton, G. Lucovsky, Y. Zhang, Y. Zou, R.J. Nemanich, H. Ade and J.L. Whitten, *J. Electron Spectrosc. Relat. Phenom.* **144** (2005), pp. 913–916.

[16] S. Zollner, Y. Liang, R.B. Gregory, P.L. Fejes, D. Theodore, Z. Yu, D.H. Triyoso, J. Curless and C. Tracy, *Am. Inst. Phys.* (2005), pp. 166–171.

[17] P. Boher, C. Defranoux, P. Heinrich, J. Wolstenholme and H. Bender, *Mater. Sci. Eng. B* **109** (2004), pp. 64–68.

[18] N.V. Nguyen, S. Sayan, I. Levin, J.R. Ehrstein, I.J.R. Baumvol, C. Driemeier, C. Krug, L. Wielunski, R.Y. Hung and A. Diebold, *J. Vacuum Sci. Technol. A* **23** (2005), pp. 1706–1713.

[19] D.H. Triyoso, R.I. Hegde, S. Zollner, M.E. Ramon, S. Kalpat, R. Gregory, X.D. Wang, J. Jiang, M. Raymond, R. Rai, D. Werho, D. Roan, B.E. White and P.J. Tobin, *J. Appl. Phys.* **98** (5) (2005), pp. 054104/1–054104/8.

[20] C. Krug and G. Lucovsky, *J. Vacuum Sci. Technol. A* **22** (2004), pp. 1301–1308.

[21] S.M. Aouadi, Y. Zhang, P. Basnyat, S. Stadler, P. Filip, M. Williams, J.N. Hilfiker, N. Singh and J.A. Woollam, *J. Phys. Condens. Matter* **18** (2006), pp. 1977–1986.

[22] C. Himcinschi, O. Gordan, G. Salvan, F. Muller, D.R.T. Zahn, C. Cobet, N. Esser and W. Braun, *Appl. Phys. Lett.* **86** (111907) (2005), p. 3 pages.

[23] E. Franke, M. Schubert, C.L. Trimble, M.J. DeVries and J.A. Woollam, *Thin Solid Films* **388** (2001), pp. 283–289.

[24] K. Hinrichs, S.D. Silaghi, C. Cobet, N. Esser and D.R.T. Zahn, *Physica Status Solidi B-Basic Solid State Phys.* **242** (2005), pp. 2681–2687.

[25] D.R.T. Zahn, S.D. Silaghi, C. Cobet, M. Friedrich and N. Esser, *Physica Status Solidi B-Basic Solid State Phys.* **242** (2005), pp. 2671–2680.

[26] S.D. Silaghi, M. Friedrich, C. Cobet, N. Esser, W. Braun and D.R.T. Zahn, *Phys. Stat. Sol. (b)* **242** (2005), pp. 3047–3052.

[27] A. Ioannidou-Philis, J.G. Philis and A.A. Christodoulides, *J. Mol. Spectrosc.* **121** (1987), pp. 50–60.

[28] L.M. Lee, R.L. Heimark, J.C. Baygents and Y. Zohar, *Nanotechnology* **17** (4) (2006), pp. S29–S33.

[29] J.A. Woollam, C.M. Herzinger, B. Johs, J.N. Hilfiker, R. Synowicki and C.L. Bungay, *Crit. Rev. Opt. Sci. Technol. CR72* (1999), pp. 29–58.

[30] H.G. Tompkins and W.A. McGahan, Spectrscopic Ellipsometry and Reflectometry: A User's Guide, Wiley-Interscience, New York (1999).

[31] J.A. Woollam, C.M. Herzinger, B. Johs, J.N. Hilfiker, R. Synowicki and C.L. Bungay, *Crit. Rev. Opt. Sci. Technol. CR72* (1999), pp. 3–28.

[32] N.V. Edwards, in: D.G. Seiler, A.C. Diebold, T.J. Shaffner, R. McDonald, S. Zollner, R.P. Khosla, E.M. Secula (Eds.), AIP, Austin, Texas (USA), 2003, pp. 723–737.

[33] V. Goossens, S. Van Gils, J. De Strycker, R. Finsy and H. Terryn, *Thin Solid Films* **493** (2005), pp. 35–40.

[34] R.A. Synowicki, *Thin Solid Films* **313–314** (1998), pp. 394–397.

[35] C.M. Herzinger, B. Johs, W.A. McGahan and W. Paulson, *Thin Solid Films* **313–314** (1998), pp. 281–285.

[36] W.H. Press, S.A. Teukolsky, W.T. Vetterling and B.P. Flannery, Numerical Recipes in C (second ed.), Cambridge University Press, New York (1992).

[37] G.E. Jellison, *Thin Solid Films* **234** (1993), pp. 416–422.

[38] A. Subramanian and W.H. Velander, *J. Mol. Recogn.* **9** (1996), pp. 528–535.

[39] E. Pretsch, P. Buhlmann and C. Affolter, Structure Determination of Organic Compounds: Tables of Spectral Data (third ed.), Springer-Verlag, New York (2000).